Pre-print of paper:
Blocken B, Carmeliet J. 2002. Spatial and temporal distribution of driving rain on a low-rise building. Wind and Structures, Vol. 5, No. 5, pp. 441-462. © TECHNO-PRESS

Spatial and temporal distribution of driving rain on a low-rise building

*Bert Blocken and Jan Carmeliet

Department of Civil Engineering
Laboratory of Building Physics
Katholieke Universiteit Leuven
Kasteelpark Arenberg 51
3001 Leuven, Belgium

*Author to whom correspondence should be addressed
Tel.: +32 (0) 16 32 13 45
E-mail: bert.blocken@bwk.kuleuven.ac.be

Abstract. This paper presents a practical numerical method to determine both the spatial and temporal distribution of driving rain on buildings. It is based on an existing numerical simulation technique and uses the building geometry and climatic data at the building site as input. The method is applied to determine the 3D spatial and temporal distribution of wind-driven rain on the facade a low-rise building of complex geometry. Distinct wetting patterns are found. The important causes giving rise to these particular patterns are identified: (1) sweeping of raindrops towards vertical building edges, (2) sweeping of raindrops towards top edges, (3) shelter effect by various roof overhang configurations. The comparison of the numerical results with full-scale measurements in both space and time for a number of on site recorded rain events shows the numerical method to yield accurate results.

Nomenclature

A_f	area of zone on building facade
A_h	area of horizontal plane in unobstructed air flow
A, n, p	constants in drop size distribution equation
d	raindrop diameter
F(d)	fraction of liquid water in the air with raindrops of diameter less than d
f	probability density of drop size distribution in the air
f_h	probability density of drop size distribution through a horizontal plane
i	number of experimental time step
j	number of numerical time step
k, l	segment numbers
n	(superscript) numerical
R_{dr}	driving rain intensity
R_h	horizontal rainfall intensity (through a horizontal plane)

S_{dr}	driving rain amount
S_h	horizontal rainfall amount (through a horizontal plane)
t	time
U, U_{10}	upstream horizontal wind velocity component at 10 m height
v_t	raindrop terminal velocity
α, β, γ	variables used in catch ratio interpolation
Δt	time interval
η_d	specific catch ratio
η	catch ratio
φ, φ_{10}	upstream wind direction at 10 m height

1. Introduction

Buildings have to provide their inhabitants and users a comfortable and healthy environment, suited to their needs. This ought to be achieved in an economically and ecologically sound way, imposing demands on the building's durability and performance. The durability and performance of building facades is governed to a large extent by moisture conditions. Driving rain or wind-driven rain is one of the most important moisture sources affecting building envelopes. Consequences of its destructive properties may take various forms. Moisture accumulation in porous materials can lead to rain penetration, frost damage, moisture induced salt migration, discolourization by efflorescence, structural cracking due to thermal and moisture gradients, to mention just a few. Driving rain impact and run-off is also responsible for rain penetration of curtain walls and for the appearance of surface soiling patterns on facades that have become characteristic for so many of our buildings (White 1967; El-Shimi et al. 1980; Mulvin and Lewis 1994; Etyemezian et al. 2000).

Information concerning the exposure to driving rain is essential in order to design building envelopes with a satisfactory hygrothermal performance. To analyse the hygrothermal behaviour of building components, Heat-Air-Moisture (HAM) transfer models are employed. They require the conversion of climatic data series (wind speed, wind direction, rainfall intensity) into accurate knowledge of the spatial and temporal distribution of driving rain loads on the outside wall under study. The attainment of this knowledge is complicated by the diversity of parameters influencing driving rain loads: the environment topology, the building geometry, the position on the building envelope, and also wind speed, wind direction, rainfall intensity and raindrop size distribution. Until recently, research on driving rain has mainly been limited to field experiments and the use of empirical formulae. As research efforts continued to reveal the inherent complexity of the problem, researchers realised that further achievements were to be found through numerical analyses.

In the past ten years, the introduction of Computational Fluid Dynamics in the area has provided new insights in the interaction between wind, rain and the building envelope. Choi (1991) developed a numerical simulation technique to determine the spatial distribution of driving rain on buildings under steady-state conditions of wind and rain. This publication and following contributions based on this technique considerably extended the existing knowledge (Choi 1993; 1994[a]; 1994[b]; Wisse 1994; Sankaran and Paterson 1995; Lakehal et al. 1995; Karagiozis and Hadjisophocleous 1996; Karagiozis et al. 1997; Choi 1997; van Mook et al. 1997; van Mook 1999[a]; 1999[b]; Hangan 1999; Etyemezian et al. 2000; Blocken and Carmeliet 2000[a]; 2000[b]). Few attempts have been made for experimental verification. Lakehal et al. (1995) compared numerical simulations for a street-canyon with experimental data for buildings of similar geometry. Van Mook (1999[a]; 1999[b]) was the first to compare numerical simulations on a building with the corresponding full-scale measurements for

selected 10-minute intervals. Hangan (1999) compared numerical simulations with wind tunnel experiments that were carried out by Surry et al. (1994). These research efforts focused on single stationary rain events, i.e. single intervals with a stationary value of wind speed, wind direction and rainfall intensity. Blocken and Carmeliet (2000[a]; 2000[b]) extended Choi's simulation technique by adding the temporal component, allowing the determination of both the spatial and temporal distribution of driving rain for transient rain events. At that time, a preliminary 2D experimental verification was conducted. A more complete 3D verification will be made in the present paper.

Despite the progress made in the past decade, there are important questions that remain unanswered. A thorough analysis of driving rain on buildings of complex geometry has not yet been performed. Neither has an experimental verification of the numerical method for transient rain events. As a result, there is no knowledge as to how well the numerical method performs in real-life situations. The objectives of the present paper are: (1) The presentation and application of the developed numerical method for spatial and temporal driving rain distribution. The application is performed for a low-rise building of complex geometry and a number of on site recorded rain events. (2) The identification of the causes for the complicated wetting patterns. (3) A full-scale experimental verification of the numerical method in both space and time.

2. Driving rain: definitions and parameters

The joint occurrence of wind and rain causes obliquity of the rain intensity vector (Fig. 1). In general, *driving rain intensity* refers to this oblique rain vector. From the viewpoint of the interaction between rain and vertical building facades, the term *driving rain intensity* takes on the narrower meaning of *component of the rain vector causing rain flux through a vertical plane*. The latter definition is used in the present paper. The other component of the rain vector, that causes rain flux through a horizontal plane, is termed (horizontal) rainfall intensity. The quantities used to describe the driving rain load are the specific catch ratio η_d, related to the raindrop diameter d, and the catch ratio η, related to the entire spectrum of raindrop diameters (Eq. (1)). They respectively correspond to the LEF (Local Effect Factor) and the LIF (Local intensity Factor) used by Choi (1994[a]).

$$\eta_d(t) = \frac{R_{dr}(d,t)}{R_h(d,t)} \quad , \quad \eta(t) = \frac{R_{dr}(t)}{R_h(t)} \tag{1}$$

where $R_{dr}(d,t)$ and $R_h(d,t)$ are the specific driving rain intensity and specific unobstructed horizontal rainfall intensity for raindrops with diameter d. $R_{dr}(t)$ and $R_h(t)$ refer to the same quantities but integrated over all raindrop diameters. The unobstructed horizontal rainfall intensity is the intensity of rainfall through a horizontal plane that is situated outside the wind flow pattern that is disturbed by the building. In practical applications the (specific) catch ratio will be measured and calculated for discrete time steps $[t_j, t_j+\Delta t]$. The (specific) catch ratio for a discrete time step is redefined as:

$$\eta_d(t_j) = \frac{\int_{t_j}^{t_j+\Delta t} R_{dr}(d,t)\,dt}{\int_{t_j}^{t_j+\Delta t} R_h(d,t)\,dt} = \frac{S_{dr}(d,t_j)}{S_h(d,t_j)} \quad , \quad \eta(t_j) = \frac{\int_{t_j}^{t_j+\Delta t} R_{dr}(t)\,dt}{\int_{t_j}^{t_j+\Delta t} R_h(t)\,dt} = \frac{S_{dr}(t_j)}{S_h(t_j)} \tag{2}$$

where $S_{dr}(d,t_j)$ and $S_h(d,t_j)$ are the specific driving rain amount and specific unobstructed horizontal rainfall amount during time step $[t_j, t_j+\Delta t]$ for raindrops with diameter d. $S_{dr}(t_j)$ and $S_h(t_j)$ again refer to the same quantities integrated over all raindrop diameters. The driving rain amount S_{dr} for each time step is obtained by multiplying the catch ratio η with the unobstructed horizontal rainfall amount S_h for this time step.

The catch ratio is a complicated function of space and time. The six basic influencing parameters for the catch ratio as defined in Eq. (2) are: (1) building geometry (including environment topology), (2) position on the building envelope, (3) wind speed, (4) wind direction, (5) (horizontal) rainfall intensity and (6) (horizontal) raindrop size distribution. In this paper, we neglect the turbulent dispersion of raindrops, the reason of which will be discussed in the next section. Reference wind speed U_{10} (m/s) and wind direction φ_{10} (degrees from north) refer to values at 10 m height in the undisturbed flow. Horizontal rainfall intensity R_h (mm/hr or L/m²hr) and horizontal raindrop size distribution $f_h(d)$ (m^{-1}) refer to values through a horizontal plane in the undisturbed flow field.

3. Numerical method for spatial and temporal driving rain distribution

3.1. Existing steady-state simulation technique

The last decade, a particular numerical simulation technique of driving rain was developed by Choi (1991) and has been employed by a large number of researchers since then. This technique is the basis for the method developed in this paper. It is a steady-state technique, comprising four steps:

(i) The steady-state wind flow pattern around the building is calculated using a CFD code.
(ii) Raindrop trajectories are obtained by injecting raindrops of different sizes in the calculated wind flow pattern and solving their equations of motion.
(iii) The specific catch ratio is determined based on the calculated raindrop trajectories.
(iv) The catch ratio is calculated from the specific catch ratio and the size distribution of raindrops.

The calculation of the specific catch ratio (η_d^n) and catch ratio (η^n) is performed for a selected number of zones on the building envelope. For each zone, the same procedure is employed. In a steady-state wind flow pattern - thus neglecting turbulent dispersion of raindrops - raindrop trajectories of diameter d ending on the corner points of the zone form a stream tube (Fig. 2). Conservation of mass for the raindrops allows η_d^n to be expressed in terms of areas:

$$\eta_d^n(d) = \frac{R_{dr}(d)}{R_h(d)} = \frac{A_h(d)}{A_f} \tag{3}$$

where A_f is the area of the zone on the building envelope where η_d^n is to be determined, and $A_h(d)$ is the area of the horizontal plane bounded by the injection positions of the raindrops of diameter d ending on the corner points of A_f. This plane A_h is located in the undisturbed wind flow. Its location must allow the raindrops injected at that position to reach their terminal velocity of fall (vertical) and the wind velocity (horizontal) before entering the flow pattern disturbed by the presence of the building. The catch ratio η^n for a zone is obtained by multiplying η_d^n for each raindrop diameter d for this zone with the fraction of these drops in the spell (raindrop size distribution $f_h(d)$) and integrating over all raindrop diameters:

$$\eta^n = \int_d f_h(d)\,\eta_d^n(d)\,\mathrm{d}d \tag{4}$$

3.2. Rain modelling considerations

As measuring *raindrop size distributions* with good accuracy is difficult – the reader is referred to the work of Salles et al. (1998; 1999) and Salles and Poesen (1999) for recent studies on this particular subject - and such data is not generally available, information on raindrop size spectra for the purpose of driving rain estimation is usually obtained from empirical formulae (Marshall and Palmer 1948; Best 1950; Mualem and Assouline 1986). For the present study, the formula of Best (1950) is adopted. This choice is based on the extent of the study carried out by Best. The study was supported by a wide bibliographical survey and measurements for a large number of rain events. His findings indicated that in many cases the size distribution of raindrops is in good accordance with Eq. (5):

$$F(d) = 1-\exp\left(-\left(\frac{d}{a}\right)^n\right), \qquad a = AR_h^{\,p}, \qquad f(d) = \frac{\mathrm{d}F}{\mathrm{d}d} \tag{5}$$

where F(d) is the fraction of liquid water *in the air* with raindrops of diameter less than d and A, n, p are parameters the experimentally determined averages of which are 1.30, 2.25, 0.232 respectively. The function f(d) yields the probability density of drop size. Due to the variation of the terminal velocity of fall of a raindrop with size, the raindrop size distribution *in the air* differs from the raindrop size distribution *through a horizontal plane*. The former can be converted to the latter by multiplying with the raindrop terminal velocity of fall:

$$f_h(d) = \frac{f(d)\,v_t(d)}{\int_d f(d)\,v_t(d)\,\mathrm{d}d} \tag{6}$$

where $f_h(d)$ represents the raindrop size distribution through a horizontal plane, f(d) the raindrop size distribution in the air and $v_t(d)$ the terminal velocity of fall of a raindrop with diameter d. Results of *raindrop terminal velocity* measurements can be found in Gunn and Kinzer (1949) and Best (1950). $f_h(d)$ is presented in Fig. 3 for various rainfall intensities. The terminal velocity of fall for raindrops as measured by Gunn and Kinzer is depicted in Fig. 4 along with the fitted curve.

Drag coefficient formulae for spherical particles (Morsi and Alexander 1972) are often used in raindrop trajectory calculations. As falling raindrops deviate from the spherical shape (Pruppacher and Klett 1978) these drag coefficients are an underestimation of the real ones, especially at high relative Reynolds numbers. High relative Reynolds numbers (referring to the airflow around an individual raindrop) are found in the case of large raindrops and/or a large difference between wind and raindrop velocity. Appropriate drag coefficients for falling raindrops were measured by Gunn and Kinzer (1949) and have been implemented in the particle tracking procedures of the authors.

The need for modelling the *turbulent dispersion of raindrops* in driving rain simulations remains an issue of disagreement amongst researchers. Lakehal et al. (1995) evaluated three turbulent dispersion models to determine the driving rain distribution in a street-canyon. Although the turbulent dispersion effect appeared weak for all but the smallest raindrops, it

was demonstrated that it can be important in some special cases (e.g. buildings completely shadowed by others giving rise to very weak upstream wind flow patterns). Sankaran and Paterson (1995) conducted simulations on a high-rise building. They found a very large influence of turbulent dispersion when looking at the driving rain amounts on large facade zones at the windward building face. With a similar building configuration and also considering large facade zones at the windward face, Etyemezian et al. (2000) found the effect of turbulent dispersion to be small. Choi (1997) performed simulations for a 40*40*40 m^3 building studying the effect of small uncorrelated gusts (0.1 s gust period) and large correlated gusts (3 s gust period). For both gust types a small influence on the mean (i.e. averaged over time) driving rain amounts on the windward face of the building was found. For large correlated gusts however a significant effect on the standard deviation of the time fluctuation of the driving rain amount was observed. The present paper will not give a definite answer to the importance of modelling turbulent dispersion, but the experimental verification performed here will show that an accurate determination of the driving rain distribution - in the building situation and at the time scale (10 minutes) considered here - can be obtained without modelling turbulent dispersion.

3.3. Numerical estimation method

3.3.1. Objective

Taking into account the rain modelling considerations, the existing steady-state simulation technique is incorporated into a generalised numerical estimation method. The objective of the numerical method is to estimate both the spatial and temporal distribution of driving rain on buildings for transient rain events. A rain event is defined here as a period of time of variable length during which it rains at least once, and that can be interspersed with periods without rainfall. The spatial distribution of driving rain is obtained by determining the driving rain load at each position of the building envelope. The temporal distribution results from performing these calculations for user defined discrete time steps. The time scale at which the climatic data samples are available is called the experimental time scale and the corresponding time step is noted as Δt^e (index i). The user defined time scale at which the catch ratio or driving rain load is calculated is called the numerical time scale and the corresponding time step is noted as Δt^n (index j). The numerical time step is larger than or equal to the experimental time step and comprises an integer number of experimental time steps. Its size is usually determined by its application (e.g. Heat, Air and Moisture simulation program: Δt^n = 1 hour or 1 day, Δt^e = 10 minutes). Fig. 5 represents a schematic of input and output data in the numerical method for driving rain estimation for Δt^e = 10 minutes and Δt^n = 1 hour.

3.3.2. Method

In the following, the discussion is limited to wind direction perpendicular to the windward facade of the building. Recalling the six basic influencing parameters for the catch ratio mentioned above, for a given building geometry, position on the building envelope and wind direction, the catch ratio is a function of wind speed, rainfall intensity and raindrop size distribution. When the raindrop size distribution of Best is adopted (Eq. (5)), a one to one relation exists between rainfall intensity and the raindrop spectrum, causing the wind speed and rainfall intensity values to unambiguously define a numerical catch ratio.

The steady-state simulation technique can be used to calculate the numerical catch ratio under steady-state conditions, i.e. for one single value of wind speed and rainfall intensity. To determine the numerical catch ratio for a transient rain event, with fluctuating wind speed and rainfall intensity, this event is partitioned into a number of equidistant time steps, each of which is considered steady-state. The time step length is taken equal to the experimental time step size Δt^e (see Fig. 5). This way, with each time step (index i), a measured value of reference wind speed U_i (= U_{10}) and horizontal rainfall intensity R_{hi} is associated. For each (experimental) time step i, the corresponding catch ratio can now be calculated by employing the steady-state technique for the couple (U_i, R_{hi}).

To reduce the computational expense, the time consuming steady-state technique will only be employed for a limited number of wind speed and rainfall intensity couples (U_i, R_{hi}), while intermediate results will be obtained by linear interpolation. Let steady-state numerical catch ratio values have been determined for a particular zone on the building envelope and for various combinations of wind speed U_{10} (U_1 ... U_k ... U_m) and rainfall intensity (R_{h1} ... R_{hl} ... R_{hn}) as presented in Fig. 6a. Let us consider an experimental time step i in the rain event and let the corresponding couple (U_i, R_{hi}) be situated in segment (k,l) as shown in Figure 6a:

$$U_k \leq U_i < U_{k+1} \quad , \qquad R_{hl} \leq R_{hi} < R_{h(l+1)} \tag{7}$$

Each segment (k,l) is characterised by four calculated values for η^n. As these values generally do not define a plane in the (U_{10}, R_h, η^n) space, the segment is split up into two partial segments $(k,l)^{(1)}$ and $(k,l)^{(2)}$ (Fig. 6b). Each of these partial segments is characterised by three η^n values that do define a plane. For each of these partial segments, this plane is used as an approximation for the actual surface $\eta^n = f(U_{10}, R_h)$. Hence, if the couple (U_i, R_{hi}) is situated in segment $(k,l)^{(1)}$, the numerical catch ratio for experimental time step i, η^n_i, is approximated by linear interpolation as follows:

$$\eta_i^n = \alpha_{kl}^{(1)} \left(U_i - U_k\right) + \beta_{kl}^{(1)} \left(R_{hi} - R_{hl}\right) + \gamma_{kl}^{(1)} \tag{8}$$

$$\alpha_{kl}^{(1)} = \frac{\eta^n_{(k+1,l)} - \eta^n_{(k,l)}}{U_{k+1} - U_k}, \quad \beta_{kl}^{(1)} = \frac{\eta^n_{(k,l+1)} - \eta^n_{(k,l)}}{R_{h(l+1)} - R_{hl}}, \quad \gamma_{kl}^{(1)} = \eta^n_{(k,l)} \tag{9}$$

If the couple (U_i, R_{hi}) is situated in segment $(k,l)^{(2)}$:

$$\eta_i^n = \alpha_{kl}^{(2)} \left(U_i - U_{k+1}\right) + \beta_{kl}^{(2)} \left(R_{hi} - R_{h(l+1)}\right) + \gamma_{kl}^{(2)} \tag{10}$$

$$\alpha_{kl}^{(2)} = \frac{\eta^n_{(k+1,l+1)} - \eta^n_{(k,l+1)}}{U_{k+1} - U_k}, \quad \beta_{kl}^{(2)} = \frac{\eta^n_{(k+1,l+1)} - \eta^n_{(k+1,l)}}{R_{h(l+1)} - R_{hl}}, \quad \gamma_{kl}^{(2)} = \eta^n_{(k+1,l+1)} \tag{11}$$

The numerical catch ratio for the numerical time step j (η^n_j) is determined from the numerical catch ratios for each of the experimental time steps i (η^n_i) that are comprised in the time step j. The numerical catch ratio for time step j is obtained by expressing that the summed driving rain amount over all the time steps i comprised in the time step j must equal the driving rain amount for time step j:

$$\sum_{i=s_j}^{e_j} \eta_i^n \, S_{hi} \quad = \quad \eta_j^n \sum_{i=s_j}^{e_j} S_{hi} \quad or \quad \eta_j^n \quad = \quad \frac{\sum_{i=s_j}^{e_j} \eta_i^n \, S_{hi}}{\sum_{i=s_j}^{e_j} S_{hi}} \tag{12}$$

where s_j and e_j are the numbers of the first and last experimental time step in numerical time step j, and S_{hi} is the horizontal rainfall amount for time step i. Combining Equation (12) with Equations (8) and (10), the numerical catch ratio for the numerical time step j can be expressed in terms of the results of the steady-state method ($\alpha_{kl}^{(1)}$, $\beta_{kl}^{(1)}$, $\gamma_{kl}^{(1)}$, $\alpha_{kl}^{(2)}$, $\beta_{kl}^{(2)}$, $\gamma_{kl}^{(2)}$) for each segment (k,l) and the experimental data (U_i, S_{hi}, R_{hi}) for each time step i.

4. Application and verification

4.1. Experimental facility

The method is applied to determine the spatial and temporal distribution of driving rain on the facade of the low-rise VLIET test building in Heverlee, Leuven. The building consists of two main modules, the flat roof module and the sloped roof module (Fig. 7). In between the main modules, there is a small terrace module. The building is 25.2 m long and 7.2 m wide. The height of flat and sloped roof module is 4.3 m and 7.9 m respectively. The terrace height is 3.95 m. Roof overhang length varies along the length axis of the building as indicated in Fig. 7. The direction of the prevailing winds at the test site is south-west. The building is situated in a suburban area. The only elements providing some shielding from wind and rain are a row of poplars at the north-west side and some low agricultural constructions that are situated about 80 m in front of the south-west facade.

Meteorological data (reference wind speed U_{10}, wind direction φ_{10}, horizontal rainfall amount S_h, horizontal rainfall intensity R_h) are gathered on site by an automatic weather station measuring on a 10 minute basis. In addition, 9 driving rain gauges are positioned on the building envelope (Fig. 7). The gauges are traditional plate type gauges made of pvc with a square (30 * 30 cm²) catch area and are fixed at the building surface. Gauges 1-6 and 8-9 are connected to reservoirs the content of which is measured manually on a daily basis. Gauge 7 is connected to a tipping bucket rain gauge measuring on a 10 minute basis to give more detailed temporal information. It is noted that a drawback of using a tipping bucket system is that the temporal resolution of the measurement is variable because it is dependent on the captured rain intensity (a tip is only given when a fixed amount of water has been collected). The tipping bucket rain gauge used here has a horizontal catch area of 507 cm² and a gauge resolution of 0.2 mm/tip. It is connected to a driving rain gauge with a larger catch area (900 cm²), thus increasing the gauge resolution from 0.2 mm/tip to 0.113 mm/tip. The effect of the resolution limit on the measurement results will be discussed later in this section.

4.2. Steady-state numerical simulations

The steady-state numerical simulation technique is employed to calculate the numerical catch ratio η^n for a selected set of couples (U_i, R_{hi}). It comprises the calculation of the wind flow pattern, the raindrop trajectories, the specific catch ratio and the catch ratio.

4.2.1. Wind flow pattern

The building model is immersed in a boundary layer flow with a logarithmic profile. Roughness length is taken 0.25 m according to the updated Davenport roughness classification (Wieringa 1992). The roughness classification was confirmed by recent measurements of the on site upstream wind speed profile at 2, 4, 6, 10 m height. The wind simulations are performed on an unstructured, tetrahedral grid with 906506 cells in a 200*90*40 m^3 computational domain using a commercial CFD code. As the standard k-ε model is known to provide inferior performance in simulating separated flows, the realizable k-ε model developed by Shih et al. (1995) was used in this study. The term "realizable" refers to mathematical constraints on the normal stresses that are satisfied by the model: positivity of normal stresses and Schwarz inequality for shear stresses. The realizable k-ε model has been validated for a wide range of flows including separated flows and has been found to perform substantially better than the standard k-ε model (Shih et al. 1995; Kim et al. 1997). The use of two-layer based non equilibrium wall functions (Kim and Choudhury 1995) is preferred to standard wall functions. The reason is their capability to partly account for the effects of pressure gradients and departure from equilibrium, which makes them more suitable for complex flows involving strong adverse pressure gradients, separation and recirculation. The steady-state wind flow pattern is calculated for reference wind speed U_{10} = 1, 2, 3, 4, 5, 6, 7, 8, 9, 10 m/s and for wind direction perpendicular to the south-west facade. Some results are given in Fig. 8a and 8b illustrating velocity vectors with their point of application in the horizontal plane at 3 m height above ground and in the vertical plane in the middle of the flat roof module respectively. The figures clearly demonstrate the wind deceleration (wind blocking) by the building and the important acceleration (speed up) of wind at the vertical and horizontal upwind building edges. These features will have a significant influence on the raindrop trajectories and the (specific) catch ratio as will be shown in the next sections.

4.2.2. Raindrop trajectories

For each of the wind flow patterns calculated, 3D Lagrangian particle tracking is performed for raindrops with diameters ranging from 0.3 to 1 mm in steps of 0.1 mm, and from 1 to 6 mm in steps of 0.2 mm. Figs. 9a and 9b show a perspective, front and top view of particle trajectories of 1 and 5 mm raindrops in the 10 m/s flow field. Fig. 10a and 10b present trajectories of raindrops that are equidistantly injected from three straight lines that are perpendicular to the south-west facade (1 and 5 mm drops, 5 m/s and 10 m/s). In general, it is observed that for smaller drops and at higher wind speed, the trajectories are more inclined and their distortion near the building becomes more pronounced. For larger drops (higher inertia) and at lower wind speed, the trajectories are less inclined and more rectilinear. In particular, three effects are identified, the first and the second of which are most pronounced for the smaller drops and at high wind speed: (1) Fig. 9: the drops are swept towards the vertical edges of the facade due to the wind acceleration in this area. (2) Fig. 9 and 10: near the flat roof module and terrace, the wind acceleration causes the drops at the upper part of the facade to be swept upwards. For the sloped roof module, this effect is clearly a lesser one given the wind blocking by the sloped roof. For both modules, a downward deflection of the trajectories of especially the smaller drops at the lower parts of the facade due to wind blocking is observed. (3) Fig. 10: the presence of roof overhang provides shelter from rain and limits the influence of the second effect. The combination of these effects causes the trajectory endpoints to be more concentrated near the vertical edges and at the upper parts of the facade that are not sheltered by roof overhang. Hence one can expect the spatial distribution to show higher driving rain amounts at these positions than say for example in the middle of the facade near the ground.

4.2.3. Specific catch ratio

The south-west building facade is divided into 40320 square zones of approximately 0.05 * 0.05 m². The specific catch ratio is calculated for each zone, for all 33 raindrop diameters and for each wind speed value. The reason for this large amount of very small zones was to obtain results with a high spatial resolution. This allows us to accurately predict the line on the facade abruptly separating sheltered and non sheltered facade areas (roof overhang). The spatial variation of the specific catch ratio for U_{10} = 5 m/s and 10 m/s and for d = 1 mm and 5 mm is presented in Figs. 11a-d. Zones sheltered from rain are coloured black. The maximum values for each module are indicated. The contour lines were drawn based on the values obtained for each of the 40320 square zones. Because each zone was attributed a constant value over its area and the data was not smoothed, the contour lines can show small jumps (over 0.05 m) from one zone to another. Following observations are made:

(1) For a given value of wind speed and raindrop diameter, the specific catch ratio is strongly influenced by the position on the building facade giving rise to a distinct wetting pattern:
   (a) The shelter effect by roof overhang evidently increases as the overhang length increases. Near the vertical edges of the sloped roof module, the sweeping effect of drops, both sidewards and upwards, diminishes the shelter effect and the line separating sheltered and non sheltered area (shelter line) shows an upward curvature. At the roof edge of the terrace, the absence of shelter gives rise to high specific catch ratio values.
   (b) In general, the specific catch ratio is larger at the facade of the flat roof and terrace module than at the facade of the sloped roof module. This is caused by the wind blocking effect, that is larger for the latter as was also demonstrated in (Blocken and Carmeliet 2000[a]).
   (c) The sweeping effect, both sidewards and upwards, causes the specific catch ratio to significantly increase towards the vertical building edges and from the lower to the upper part of the facade. The highest values occur at the top and side edges, and, if roof overhang is present, just below the abrupt transition from sheltered to non sheltered area.

(2) Focusing on a given set of positions on the facade, wind speed and raindrop diameter have an appreciable effect on the specific catch ratio:
   (a) The shelter provided by roof overhang decreases as wind speed increases, as the trajectories are more inclined and the sweeping effect becomes more important. In general, shelter also decreases as the raindrop diameter decreases, although this is less pronounced than the influence of wind speed.
   (b) The specific catch ratio at the top and side edges strongly increases with increasing wind speed and decreasing raindrop diameter.
   (c) The spatial uniformity of driving rain on the facade decreases as the wind speed increases and the raindrop diameter decreases. This is clearly shown by the number of contour lines displayed in each figure.

Zooming into two selected positions at the facade (positions 1 and 3, corresponding to the positions of the driving rain gauges, see Fig. 7), the dependency of the specific catch ratio on wind speed and raindrop diameter can be represented as in Fig. 12a and 12b. It is noted that "position" refers to the 0.3*0.3 m² area of the driving rain gauge and thus comprises 36 small 0.05*0.05 m² zones. η_d^n significantly increases with increasing wind speed and shows a steep

increase for small diameters and high wind speed. The effect of roof overhang for position 1 is noticed as a complete cut-off for $U_{10} < 4$ m/s. For position 3, that is situated at a lower part of the facade, shelter is less pronounced. For position 1, the largest η_d^n values occur with raindrop diameters of about 1 to 2 mm, caused by the sweeping effect (Fig. 9 and 10). For both position 1 and 3, η_d^n remains approximately constant for d > 2-3 mm. The reason is to be found in drop physics. As the deformation of a falling raindrop increases with its size (Pruppacher and Klett 1978), its drag coefficient also shows an additional increase. Despite their larger mass, the terminal velocity of fall for large drops will therefore be reaching an asymptote (see Fig. 4). Furthermore, the horizontal velocity of all drop sizes in the upstream undisturbed flow approximately equals the horizontal wind velocity. As the trajectory inclination is determined by the magnitude of the raindrop horizontal and vertical terminal velocity, all large drops approach the building with more or less the same inclination. The lack of distortion of the large raindrop trajectories near the building subsequently is responsible for them having similar specific catch ratio values.

4.2.4. Catch ratio

Adopting the raindrop size distribution according to Best and thus relating the raindrop size distribution to the horizontal rainfall intensity, the numerical catch ratio can be determined for all zones as a function of wind speed and rainfall intensity by Eq. (4). The catch ratio obtained for position 1 and 3 is presented in Fig. 12c and 12d. The effect of wind speed and roof overhang is very important. The effect of rainfall intensity seems to be rather small for moderate to high rainfall intensities ($R_h > 3$ mm/hr). The reason is that for these intensities, the contribution of large drops in the raindrop size distribution becomes more and more important (Fig. 3). The larger drops all have approximately the same high specific catch ratio value – as was shown before – and thus a high weighting factor in Eq. (4) and therefore dominate the value of the catch ratio.

4.3. Rain event

The numerical method is first applied for the rain event that was recorded during 5-6 January 1998. The record of wind speed, wind direction and rainfall intensity is given in Fig. 13. The rain event consists of a continuous shower lasting more than 4 hours followed by some minor spells. The wind direction during rain was in good approximation perpendicular to the south-west building facade (225° from north). Measurements of the driving rain amounts during and at the end of the rain event were made. Until recently, knowledge concerning the accuracy of driving rain gauges was not available. Innovative experimental studies on driving rain gauge accuracy have been performed by Kragh (1998), van Mook (1998) and Högberg et al. (1999), indicating that errors in measuring driving rain can be very large. Based on these studies a numerical model was developed (Blocken et al. 2001; Blocken and Carmeliet 2001) to estimate the error in driving rain measurements. Apart from their dependence on material, size and shape of the gauge catch area, errors were found to largely depend on the type of rain event. In the interest of brevity, we limit ourselves to just mentioning the errors for the rain events studied here. Because they have to serve for experimental verification, the rain events in this paper were selected for small measurement errors.

Determining the spatial and temporal distribution of driving rain on the facade for the rain event is based on the knowledge of the 40320 surface plots describing the catch ratio for each zone as a function of wind speed and rainfall intensity (see Fig. 6 and Fig. 12c and 12d). The

experimental time step is 10 minutes (measurement interval), the numerical time step is also - arbitrarily - taken as 10 minutes.

4.4. Spatial distribution of driving rain

The spatial distribution of driving rain on the facade calculated at the end of the rain event is given in Fig. 14a. Multiplying these catch ratio values with the total horizontal rainfall amount for the rain event (S_h = 13.6 mm) yields the driving rain amount. In addition to the contour lines, the calculated catch ratio values at the positions of the driving rain gauges are given. A distinct wetting pattern is found. The observations to be made are approximately the same as made before (section 4.2.3.): sweeping effect causing highest values near the vertical and roof edges, higher values for the flat roof module, etc. An important difference to be mentioned is the disappearance of the abrupt transition (shelter line) between sheltered and non sheltered areas. The reason is twofold: (1) the presence of raindrops of different diameters in the rain event, all with a shelter line at a slightly different location and (2) the fluctuations in wind speed during the rain event, causing the shelter line for each of the raindrop diameters to move vertically across the facade as a function of time. The same reason is responsible for the position of the maximum catch ratio value at the vertical building edges: it is no longer situated just below the sheltered area but somewhat lower on the facade.

The validity of the results is ascertained by comparing the numerical results (at gauge positions 1 – 9) with the corresponding full-scale measurements (Fig. 14b). The catch ratio measurement error is about 0.02. The comparison in general shows a good agreement. Some discrepancies are observed at the edges, especially at gauge positions 1 and 2. These are the most difficult positions because of the combination of the sweeping effect of drops (sidewards and upwards) and the shelter effect by overhang at these positions. The catch ratio at gauge position 1 is most difficult to predict because it is positioned exactly on the transition region between sheltered and non sheltered area where a high wetting gradient is present (see Fig. 14a). Two remarks: (1) the measurement value in the middle of the facade was lost due to air pressure build-up in the reservoir prohibiting the driving rain water to be collected. (2) the numerical method predicts no driving rain on the north-west facade, whereas the measurements show a small amount of rain at position 9. The authors think that this can be attributed to the combined effect of the small wind direction fluctuations around 225° during the rain event and the turbulent dispersion of raindrops, not accounted for in the model. Both effects appear to have only a limited influence.

4.5. Temporal distribution of driving rain

The temporal distribution of driving rain is studied by focusing on gauge position 7. The cumulative driving rain amount (mm or L/m²) at this position during the rain event is given in Fig. 15. It is shown that the largest 10 minute driving amounts occur during the co-occurrence of higher wind speed values and peak rainfall intensities (see Fig. 13). The comparison with the measurements reveals a good agreement for the temporal variations although a small underestimation by the numerical method is to be noted. Due to the limited resolution of the tipping bucket registration system (0.113 mm/tip) only amounts that are multiples of 0.113 mm could be registered and presented in the cumulative plot. This however only appears to be a drawback when the rainfall intensity is low, as is the case in this rain event from time step i = 48 to i = 144 (Fig. 13), where finer measurements would be useful.

Fig. 16a and 16b present an additional verification of the method for two other rain events. Given the resolution limit of the tipping bucket system, these rain events also were chosen for sufficiently high rainfall intensities. Measurements errors at the end of the rain events are 0.8

mm and 0.2 mm respectively. The satisfactory agreement found earlier is confirmed by these results.

5. Conclusions

- A 3D numerical method has been presented to determine the spatial and temporal distribution of driving rain on buildings based on the building geometry and the climatic data at the building site.
- The simulation of driving rain on a low-rise building of complex geometry has revealed distinct wetting patterns. Three particular causes for these patterns have been identified: (1) sweeping of raindrops towards vertical building edges, (2) sweeping of raindrops towards top edges, (3) shelter effect by various roof overhang configurations. Consequently, the building facade positions that receive the largest amounts of driving rain are the top edges (when no roof overhang is present) and side edges. When roof overhang is present, the largest amounts occur below the sheltered area, where a high wetting gradient is present.
- The numerical results for spatial and temporal driving rain distribution were experimentally verified. In both cases a satisfactory agreement was obtained. It is noted that the current study was limited to wind direction perpendicular to the south-west facade. The current results provide a basis for further verification efforts that will take into account varying wind directions.

The important assumptions adopted for the present study are:

- The raindrop size distribution according to Best. Although this formula is based on an extensive study for a large number of rain events, deviations from the prescribed spectra are likely to occur. It was shown though that the variation of the specific catch ratio with drop size is limited to the smaller drop sizes and that their specific catch ratio does not have a large contribution to the catch ratio for moderate to high rainfall intensities. This might indicate that the sensitivity to raindrop spectra is rather small and that the knowledge of the exact raindrop size distribution is a lesser problem. Further research is required to verify this.
- Turbulent dispersion was not modelled. It has appeared that in the situation under study, accurate results can be obtained without including turbulent dispersion. Recalling the findings of Choi (1997), turbulent dispersion has a small effect on the mean driving rain amounts but there can be a significant influence of e.g. 3s duration gusts on short term driving rain fluctuations. The authors think that the use of 10 minute time steps in the present study represents a “mean” situation, as this frequency (1/600 Hz) is well below the bulk of gust frequencies in the micrometeorological peak of the wind speed power spectrum (Van der Hoven 1957). Measurements of driving rain at higher frequencies might indicate the effects found by Choi, although in doing so one must keep in mind the measurement limitations (delay in the collection of driving rain water from the gauge surface).

Further research will include:

- Increasing both the spatial and temporal measurement resolution by using more driving rain gauges and replacing the tipping bucket system by a high accuracy pressure sensor.
- A sensitivity analysis focused on the raindrop size distribution.
- Application of the numerical method to other buildings in other environment topologies.

Acknowledgements

This research is funded by the government of Flanders. As a Flemish government institution, IWT (= Institute for the Promotion of Innovation by Science and Technology in Flanders) supports and stimulates industrial research and technology transfer in the Flemish industry.

References

Best, A.C. (1950), "The size distribution of raindrops", *Q. J. Roy. Meteor. Soc.*, **76,** 16-36.

Blocken, B., and Carmeliet, J. (2000[a]), "Driving rain on building envelopes – I, numerical estimation and full-scale experimental verification", *Journal of Thermal Env. & Bldg. Sci.*, **24**(1) 61-85.

Blocken, B. and Carmeliet, J. (2000[b]), "Driving rain on building envelopes – II, representative experimental data for driving rain estimation", *Journal of Thermal Env. & Bldg. Sci.*, **24**(2) 89-110.

Blocken, B., Van Mook, F.J.R., Hagentoft, C.-E., Carmeliet, J. 2001. "A status report of numerical-experimental driving rain studies on 3 full-scale buildings", *Proceedings of 3EACWE*, Eindhoven, The Netherlands, 133-140.

Blocken, B. and Carmeliet, J. (2001), "A review on driving rain research in building science", submitted to *Journal of Thermal Env. & Bldg. Sci*.

Choi, E.C.C. (1991), "Numerical simulation of wind-driven-rain falling onto a 2-D building", *Asia Pacific Conference on Computational Mechanics*, Hong Kong, 1721-1728.

Choi, E.C.C. (1993), "Simulation of wind-driven-rain around a building", *J. Wind Eng. Ind. Aerod.*, **46**&**47**, 721-729.

Choi, E.C.C. (1994[a]), "Determination of wind-driven-rain intensity on building faces *J. Wind Eng. Ind. Aerod.*, **51**, 55-69.

Choi, E.C.C. (1994[b]), "Parameters affecting the intensity of wind-driven rain on the front face of a building", *J. Wind Eng. Ind. Aerod.*, **53**, 1-17.

Choi, E.C.C. (1997), "Numerical modelling of gust effect on wind-driven rain", *J. Wind Eng. Ind. Aerod.*, **72**, 107-116.

El-Shimi, M., White, R. and Fazio, P. (1980), "Influence of facade geometry on weathering", *Can. J. Civil Eng.*, **7**(4) 597-613.

Etyemezian, V., Davidson, C.I., Zufall, M., Dai, W., Finger, S. and Striegel, M. (2000), "Impingement of raindrops on a tall building", *Atmos. Environ.*, **34**, 2399-2412.

Gunn, R. and Kinzer, G.D. (1949), "The terminal velocity of fall for water droplets in stagnant air", *J. Meteor.*, **6**, 243-248.

Hangan, H. (1999), "Wind-driven rain studies. A C-FD-E approach", *J. Wind Eng. Ind. Aerod.*, **81**, 323-331.

Högberg, A.B., Kragh, M.K., and van Mook, F.J.R. (1999), "A comparison of driving rain measurements with different gauges", *Proceedings of 5th Symposium on Building Physics in the Nordic Countries*, Gothenburg, August, 361-368.

Lakehal, D., Mestayer, P.G., Edson, J.B., Anquetin, S., and Sini, J.-F. (1995), "Eulero-Lagrangian simulation of raindrop trajectories and impacts with the urban canopy", *Atmos. Environ.*, **29**(23) 3501-3517.

Karagiozis, A. and Hadjisophocleous, G. (1996), "Wind-driven rain on high rise buildings", *Thermal Performance of the Exterior Envelopes of Buildings VI/Moisture II*, Clearwater, Florida, December.

Karagiozis, A., Hadjisophocleous, G., and Cao, S. (1997), "Wind-driven rain distributions on

two buildings", *J. Wind Eng. Ind. Aerod.*, **67**&**68**, 559-572.
Kim, S-E. and Choudhury, D. (1995), "A near-wall treatment using wall functions sensitized to pressure gradient", *ASME FED Vol. 217, Separated and Complex Flows.*
Kim, S-E., Choudhury, D. and Patel B. (1997), "Computations of complex turbulent flows using the commercial code FLUENT", *Proceedings of the ICASE/LaRC/AFOSR Symposium on Modelling Complex Turbulent Flows*, Hampton, Virginia.
Kragh, M.K. (1998). *Microclimatic conditions at the external surface of building envelopes*. Ph.D thesis, Department of Buildings and Energy, Technical University of Denmark.
Marshall, J.S. and Palmer, W. Mck. (1948), "The distribution of raindrops with size", *J. Meteor.*, **5**, 165-166.
Morsi, S.A. and Alexander, A.J. (1972), "An investigation of particle trajectories in two-phase flow systems", *J. Fluid Mech.*, **55**(2) 193-208.
Mualem, Y. and Assouline, S. (1986), "Mathematical model for rain drop distribution and rainfall kinetic energy", *T ASAE*, **29**(2) 494-500.
Mulvin, L. and Lewis, J.O. (1994), "Architectural detailing, weathering and stone decay", *Build. Environ.*, **29**(1) 113-138.
Pruppacher, H. and Klett, J. (1978). *Microphysics of clouds and precipitation*, D. Reidel, Boston.
Salles, C., Creutin, J.D. and Sempere-Torres, D. (1998), "The optical spectropluviometer revisited", *J. Atmos. Ocean. Tech.*, **15**(5) 1215-1222.
Salles, C. and Poesen, J. (1999), "Performance of an optical spectro pluviometer in measuring basic rain erosivity characteristics", *J. Hydrol.*, **218**, 142-156.
Salles, C., Poesen, J. and Borselli, L. (1999), "Measurement of simulated drop size distribution with an optical spectro pluviometer: sample size considerations", *Earth Surf. Proc. Land.*, **24**(6), 545-556.
Sankaran, R. and Paterson, D.A. (1995), "Computation of rain falling on a tall rectangular building", *Proceedings of 9ICWE*, New Delhi, India.
Shih, T-H., Liou, W.W., Shabbir, A. and Zhu, J. (1995), "A new k-ε eddy-viscosity model for high Reynolds number turbulent flows – model development and validation", *Comput. Fluids*, **24**(3) 227-238.
Surry, D., Inculet, D.R., Skerlj, P.F., Lin, J-X., and Davenport, A.G. (1994), "Wind, rain and the building envelope: a status report of ongoing research at the University of Western Ontario", *J. Wind Eng. Ind. Aerod.*, **53**, 19-36.
Van der Hoven, I. (1957), "Power spectrum of horizontal wind speed in the frequency range from 0.0007 to 900 cycles per hour", *J. Meteorol.*, **14**, 160-164.
Van Mook, F.J.R., De Wit, M.H. and Wisse, J.A. (1997), "Computer simulation of driving rain on building envelopes", *Proceedings of 2EACWE*, Genova, Italy, 1059-1066.
Van Mook, F.J.R. (1998), "Measurements of driving rain by a driving-rain gauge with a wiper", *CIB taskgroup 21 meeting*, Gävle, Sweden, June.
Van Mook, F.J.R. (1999[a]), "Full-scale measurements and numeric simulations of driving rain", *Proceedings of 10th ICWE*, Copenhagen, Denmark, 1145-1152.
Van Mook, F.J.R. (1999[b]), "Measurements and simulations of driving rain on the Main Building of the TUE", *Proceedings of 5th Symposium on Building Physics in the Nordic Countries*, Gothenburg, Sweden, 377-384.
White, R.B. (1967). *The changing appearance of buildings*. Her Majesty's Stationery Office, London, 64 p.
Wieringa, J. (1992), "Updating the Davenport roughness classification", *J. Wind Eng. Ind. Aerod.*, **41-44**, 357-368.
Wisse, J.A. (1994), "Driving rain, a numerical study", *Proceedings of 9th Symposium on*

Building Physics and Building Climatology, Dresden, September.

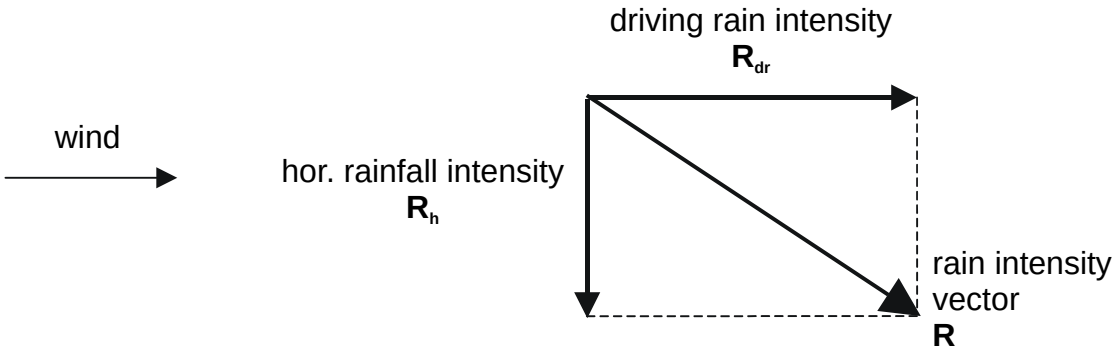

Fig. 1. Rain intensity vector R and its components: driving rain intensity R_{dr} and horizontal rainfall intensity R_h.

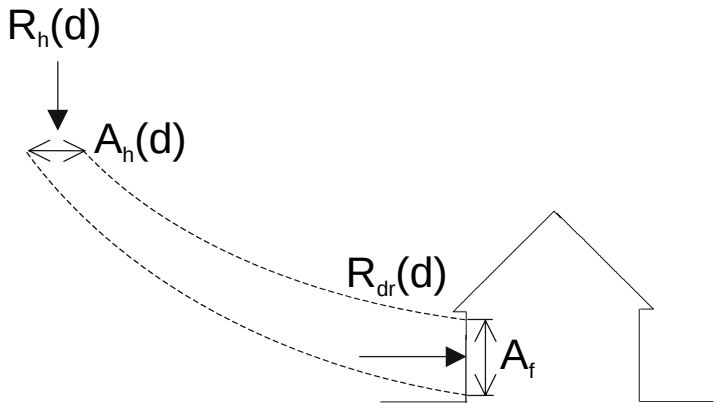

Fig. 2. Stream tube bounded by raindrop trajectories – determination of the numerical specific catch ratio for raindrops with diameter d based on conservation of mass for the raindrops.

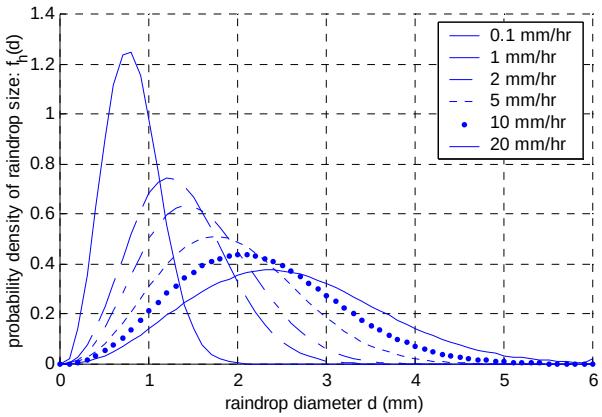

Fig. 3. Raindrop size distribution through a horizontal plane with the rainfall intensity as a parameter - calculated from raindrop size distribution in the air according to Best (1950).

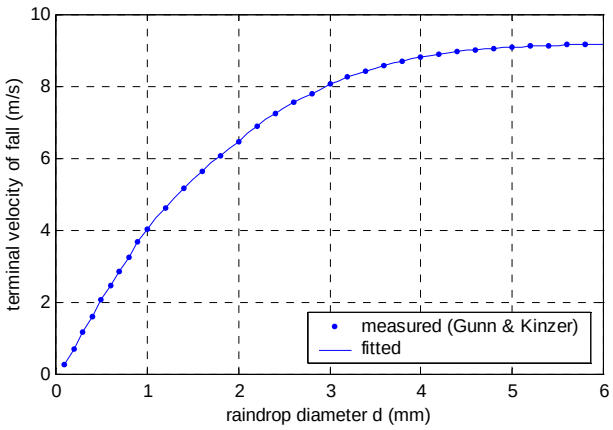

Fig. 4. Terminal velocity of fall for raindrops. Measurements by Gunn and Kinzer (1949) and fitted curve.

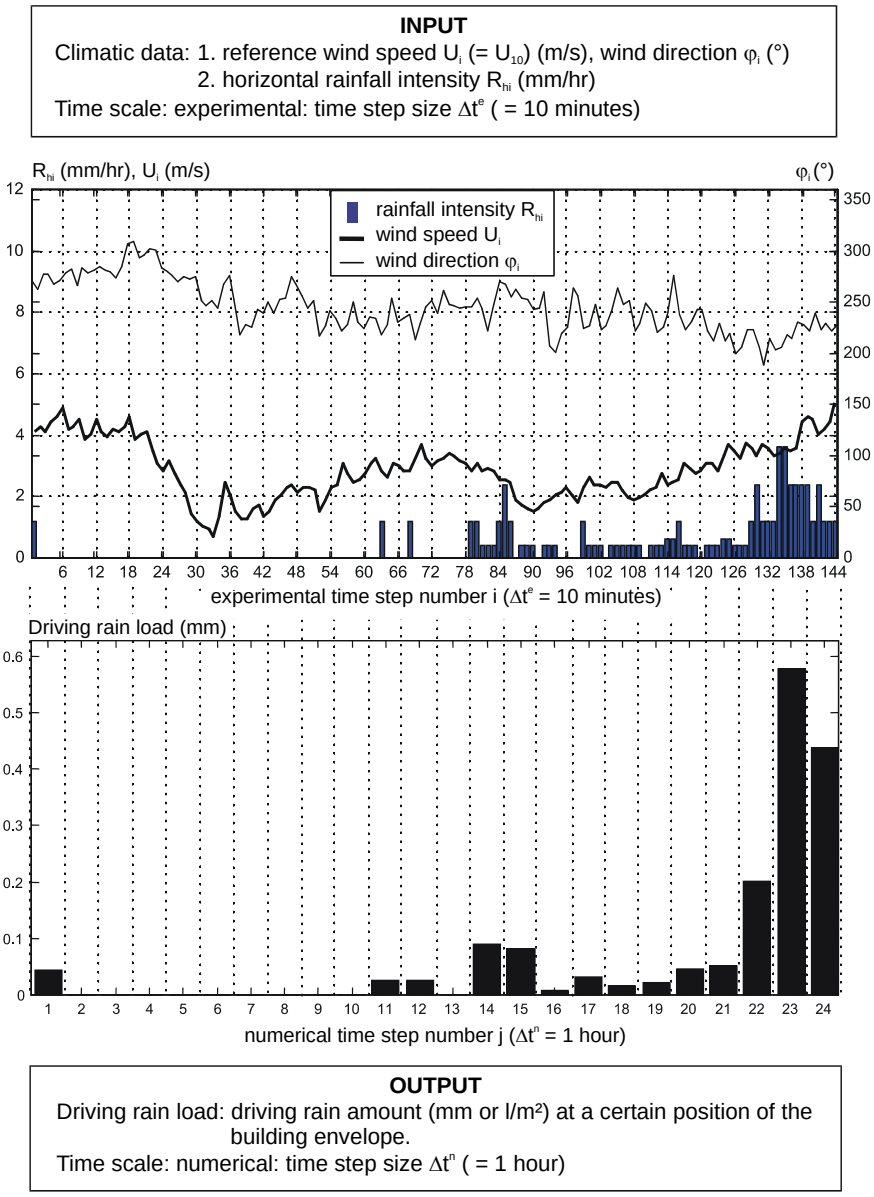

Fig. 5. Schematic representation of input and output data in the numerical method for driving rain estimation.

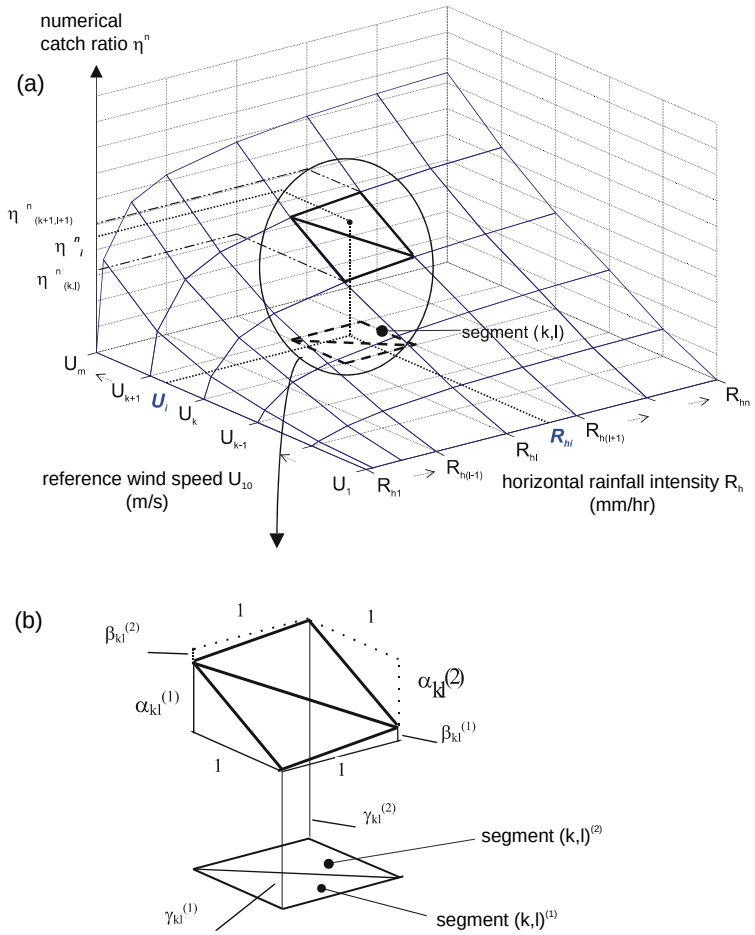

Fig. 6. (a) Example graph of the numerical catch ratio for a zone on the building envelope as a function of discrete values of reference wind speed and horizontal rainfall intensity. (b) Intermediate values are obtained by linear interpolation in triangular planes.

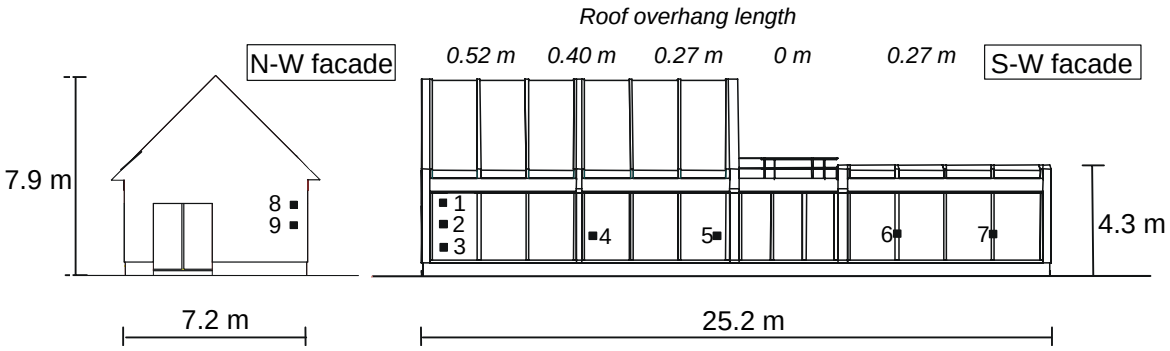

Fig. 7. VLIET test building. North-west and south-west facade. Building dimensions, roof overhang length, positions and numbers of the driving rain gauges.

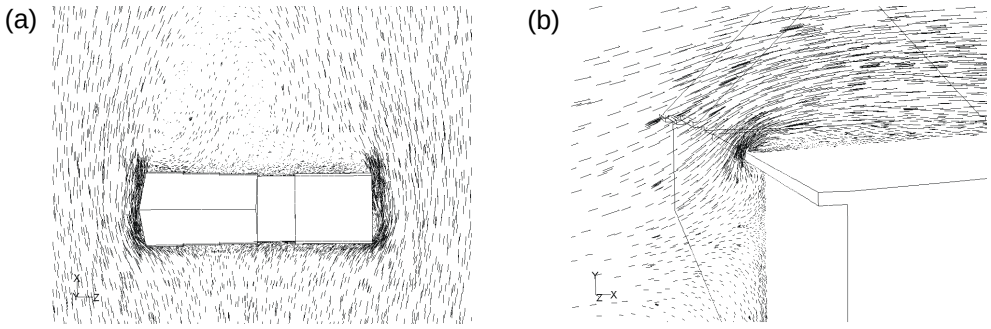

Fig. 8. Wind flow pattern. (a) Velocity vectors with point of application in the horizontal plane at 3 m above ground (b) Velocity vectors with point of application in the vertical plane in the middle of the flat roof module. Wind direction is perpendicular to the south-west facade.

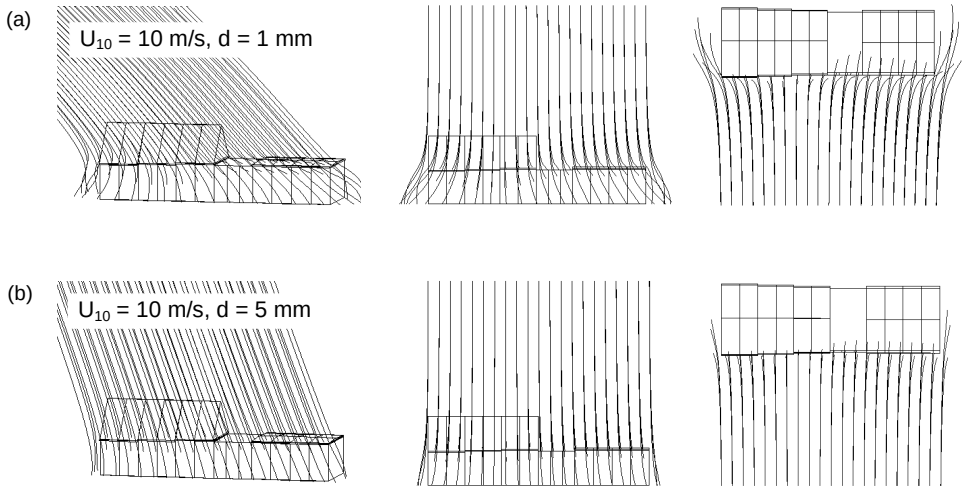

Fig. 9. Perspective, front and top view of raindrop trajectories in the U_{10} = 10 m/s wind flow pattern (a) raindrop diameter d = 1 mm, (b) raindrop diameter d = 5 mm. Wind direction is perpendicular to the south-west facade.

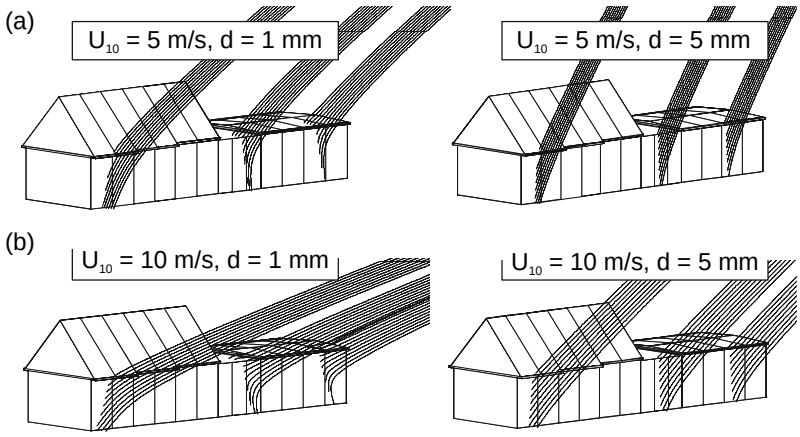

Fig. 10. (a) Raindrop trajectories (d = 1 mm, d = 5 mm) in the U_{10} = 5 m/s wind flow pattern. (b) Raindrop trajectories (d = 1 mm, d = 5 mm) in the U_{10} = 10 m/s wind flow pattern. Wind direction is perpendicular to the south-west facade. The raindrops are injected equidistantly from three straight lines that are perpendicular to the south-west facade.

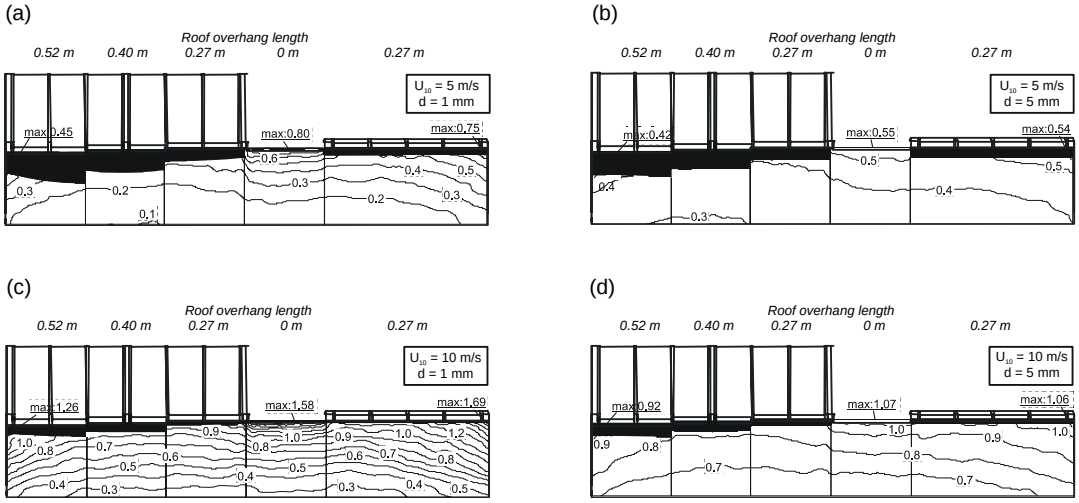

Fig. 11. Numerical specific catch ratio at the south-west facade for different values of wind speed and raindrop diameter. Wind direction is south-west (perpendicular to the facade). Areas that are sheltered from rain are coloured black. Maximum values for each module are indicated. (a) U_{10} = 5 m/s, d = 1 mm, (b) U_{10} = 5 m/s, d = 5 mm (c) U_{10} = 10 m/s, d = 1 mm (d) U_{10} = 10 m/s, d = 5 mm.

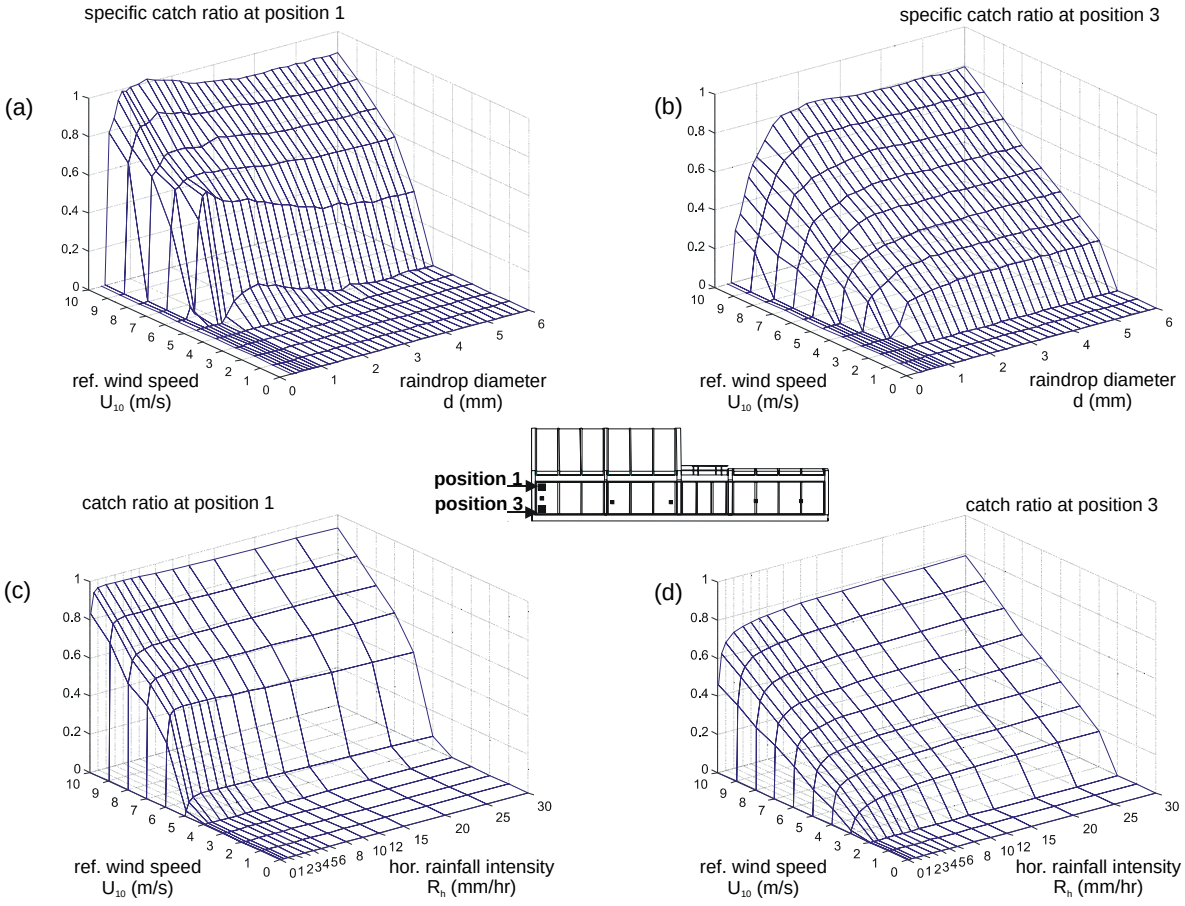

Fig. 12. (a-b) Numerical specific catch ratio η_d^n as a function of reference wind speed U_{10} and raindrop diameter d for (a) position 1 and (b) position 3 at the south-west facade. (c-d) Numerical catch ratio η^n as a function of reference wind speed U_{10} and horizontal rainfall intensity R_h for (c) position 1 and (d) position 3. Wind direction is perpendicular to the south-west facade.

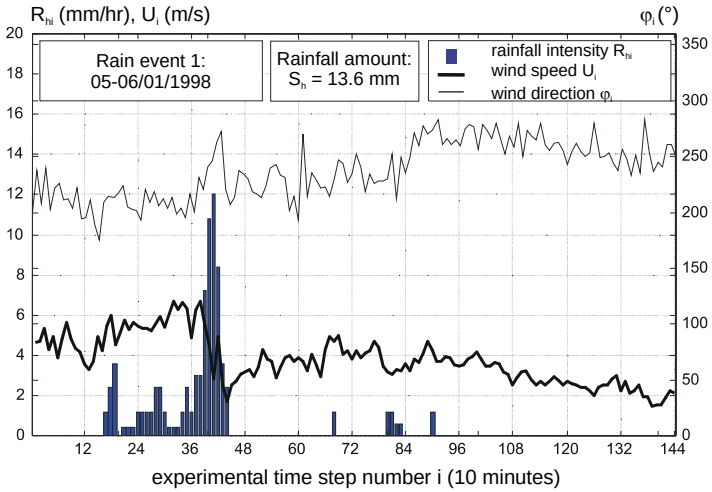

Fig. 13. Measurements of wind speed U_i, wind direction φ_i and rainfall intensity R_{hi} for each experimental time step i in the 1 day rain event (05-06/01/1998). Total horizontal rainfall amount: 13.6 mm.

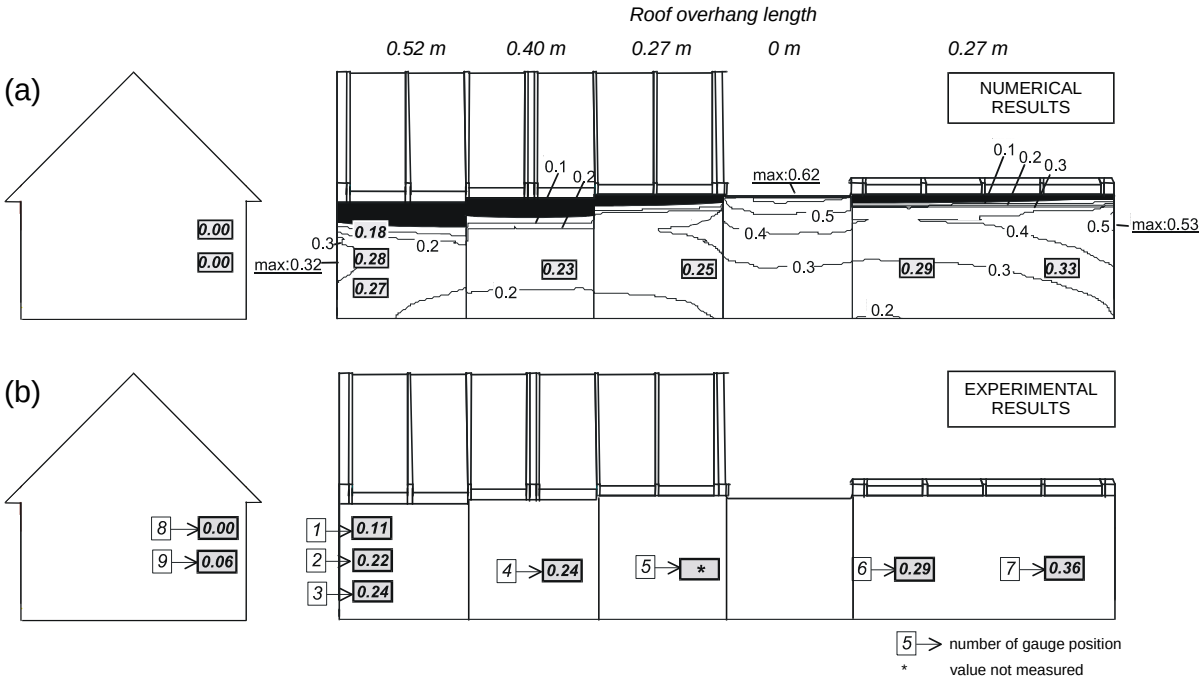

Fig. 14. (a) Numerical results for the spatial distribution of driving rain at the end of the rain event. Wind direction is south-west (perpendicular to the facade). Contour lines of the numerical catch ratio are displayed. Their values at the positions of the driving rain gauges are additionally indicated. (b) Experimental results: catch ratio measured at the end of rain event 1 (05-06/01/1998) at 9 positions.

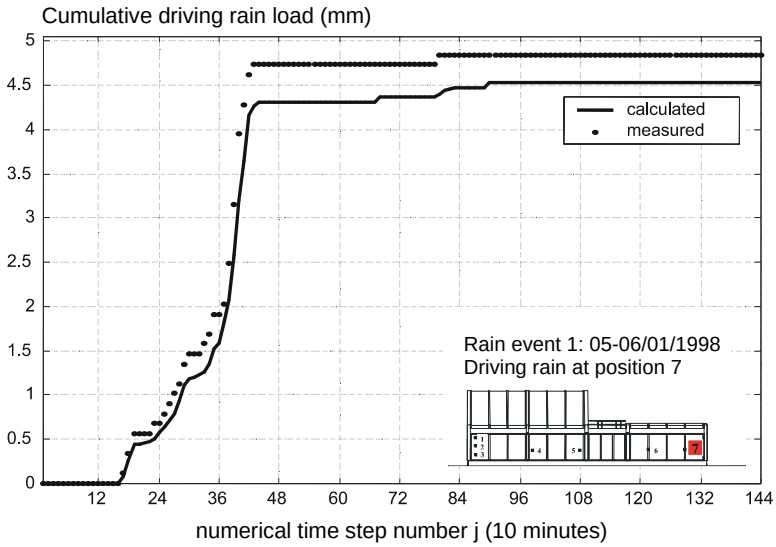

Fig. 15. Temporal distribution of the experimentally and numerically determined driving rain amount during rain event 1 (05-06/01/1998) at gauge position 7.

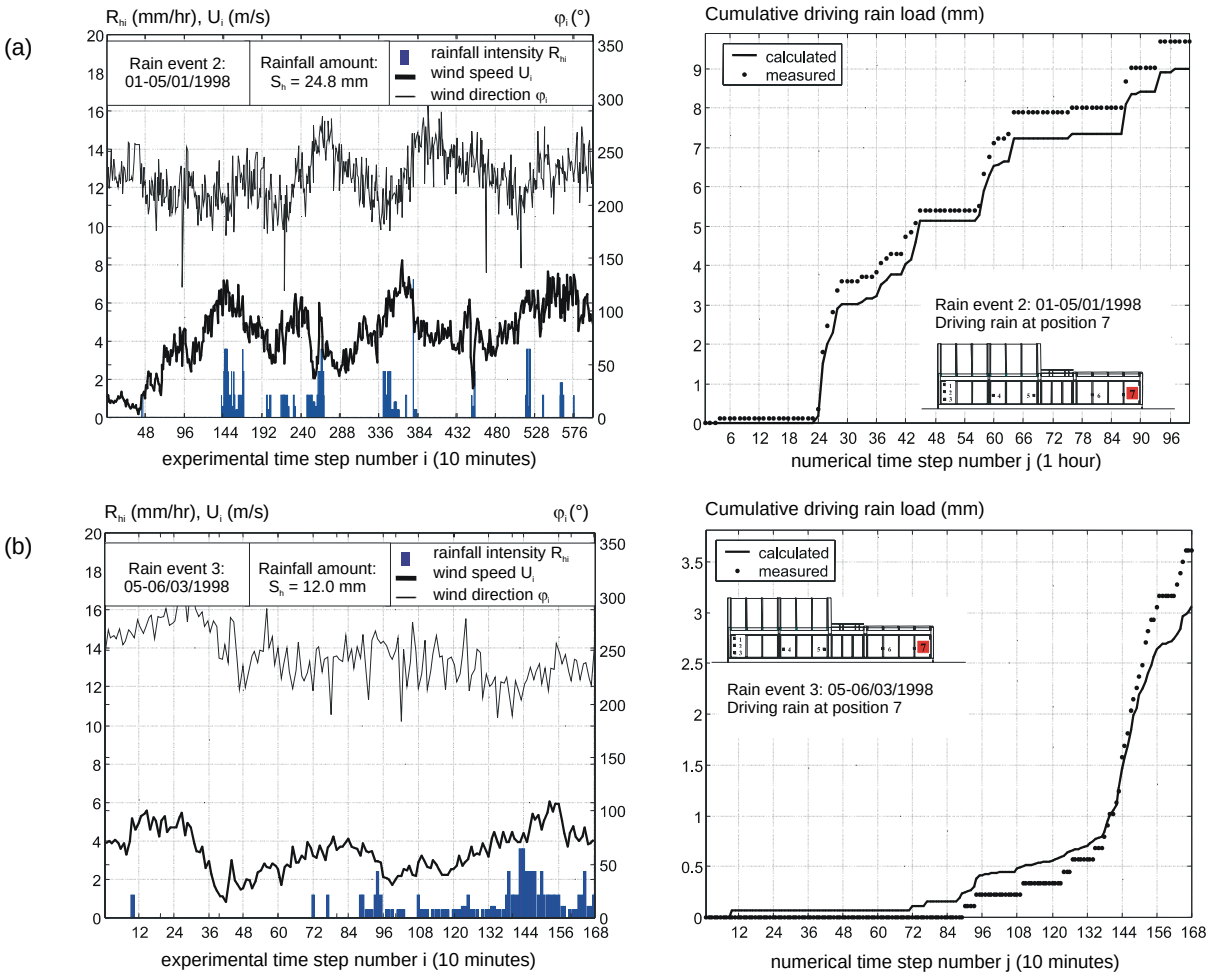

Fig. 16. Rain events and the corresponding experimentally and numerically determined temporal distribution of driving rain at gauge position 7. (a) Rain event 2 (01-05/01/1998), (b) Rain event 3 (05-06/03/1998).